ORIGINAL ARTICLE

Experimental evaluation on the axial crushing performance of BFRP-bamboo winding composite hollow components

Haitao Li [a,b,c,*], Wenjing Zhou[a], Bingyu Jian[a], Xinqi Shen[a], Rodolfo Lorenzo[d], Mahmud Ashraf[e]

[a] College of Civil Engineering, Nanjing Forestry University, Nanjing 210037, China.
[b] National-provincial joint engineering research center of biomaterials for MACHINERY PACKAGE, Nanjing Forestry University, Nanjing 210037, China.
[c] Jiangsu Engineering Research Center of Bamboo and Wood Carbon Fixation Materials and Structures, Nanjing Forestry University, Nanjing 210037, China.
[d] University College London, London WC1E 6BT, UK.
[e] Deakin University, Geelong Waurn Ponds, VIC 3216, Australia.
*Corresponding author: Haitao Li, Professor, E-mail: lhaitao1982@126.com

Abstract: In order to study the quasi-static axial crushing performance of BFRP-bamboo winding composite hollow components, considering the cloth ratio of BFRP (0%~14.68%) the number of BFRP layers (0 layer~4 layers) as an influencing factor, 20 tube specimens were designed for quasi-static compression tests. In this paper, the failure modes of the specimens under quasi-static axial compressive load are presented with the relevant load-displacement curves. The deformation types were carefully studied to evaluate the compressive crushing indicators of the specimens. The test results showed that when the cloth ratio of BFRP increased from 0 to 14.68%, the specific energy absorption (SEA), the mean crushing force (MCF) and the crushing load efficiency (CFE) increased to some extent, whilst the initial peak crushing force (PCF) did not show any trend. When compared with those of the bamboo winding hollow components (BT), the SEA, MCF and CFE of BFRP-bamboo winding composite hollow components with four layers of BFRP winding outside of BT (BBT4) increased by 87.53%, 194.37% and 255.59% respectively. Compared with other composite hollow components such as composite wrapped hollow components (CWT) and carbon reinforced composite hollow components (CRCT), BFRP-bamboo winding composite hollow components (BBT) showed superior crushing resistance while offering the advantages of light weight.

Keywords: Bamboo winding composite materials; hollow components; energy absorption; failure analysis

1 Introduction

Bamboo is known as a natural green building material [1, 2] offering high strength-to-weight ratio, and plays a vital role in structural application [3, 4]. With the development of science and technology, many different kinds of engineered bamboo products were invented, such as laminated bamboo lumber (also named glued laminated bamboo), parallel bamboo strand lumber (also named scrimber bamboo), GluBam, bamboo winding composite material, bamboo chip composite material, bamboo plastic composite material, bamboo wood composite material, bamboo straw composite material and so on [3]. Engineered bamboo products can partly replace traditional concrete, metal or plastic in different

engineering area and our everyday life, which will effectively reduce the use of mineral products reducing the demand for high energy consumption products and eventually save resources and thus protect the environment [3-7].

As for bamboo winding composite material, it was invented firstly by Chinese scientists from Chinese Academy of Forestry and Nanjing Forestry University in 1950's, and bamboo curtain or bamboo mat was used as the winding element then [8]. Ye et al. [9-11] has done a lot of research on bamboo winding composite tubes made of bamboo curtains. Li et al. [3, 12-15] invented many manufacturing methods for bamboo winding composites components with bamboo veneer or bamboo skin in 2008. Since 2008, Li et al. [3, 12-15] continued the research on bamboo winding composite materials, developing a series of products leading to obtaining more than 60 patents with different kinds of winding elements such as bamboo curtain (bamboo mat), bamboo veneer or bamboo skin and so on. The bamboo winding hollow components developed by his research team, in various diameters, can be applied in civil engineering, transportation, water conservancy, and other infrastructure construction fields, as shown in **Fig. 1**.

| (a) | (b) |

Fig. 1. Bamboo winding composite hollow components of different diameters.

Basalt fiber reinforced polymer (BFRP) is an environmental-friendly building material [16]. Wrapping BFRP on the outside of traditional materials has been shown to improve the durability of the material while enhancing its strength and ductility [17]. Previous studies on fiber reinforced metal hollow components and fiber reinforced plastic hollow components have clearly demonstrated that they have excellent crushing resistance [18, 19] which led to their wide usage in aerospace, automotive industry and other construction industries [20, 21].

Researchers from across the world have done significant research on the quasi-static axial crushing properties of traditional metal hollow components or fiber reinforced composite hollow components. They explored the failure characteristics and crushing resistance of specimens by considering factors such as section shape [22-24], loading mode [25-27] and stacking direction [28].

No significant research has been reported on the quasi-static axial crushing performance of bamboo or winding wood circular hollow components. Li et al. [14] investigated the axial compressive behaviour of transversely reinforced bamboo winding tubes. Research has shown that bamboo winding hollow components, when reinforced transversely, exhibit significant improvements in axial compressive strength and ductility, making them suitable for structural applications, where high compressive strength is required [14]. Jian et al.[15] have demonstrated that the winding angle of bamboo tubular sections plays a crucial role in their compression properties. By varying the winding angle, the structural integrity and energy absorption capacity of bamboo winding hollow components can be optimized; this clearly highlights the importance of careful design considerations in bamboo composite materials. Zhang et al. [29] carried out the ring stiffness test of winding bamboo composite pipe; the results showed that the ring stiffness of pipe at the connection is greater than that of the header pipe. Ma et al. [30] carried out the bending strength test of winding bamboo composite pipe. The bending strength difference between the two methods showed that the bending strength of the axial

specimen much higher. Wei et al. [31] studied the axial compression properties of bamboo composite tubes, analyzed the stress-strain relationship based on the continuous strength design method. Gu dou et al. [32] compared the SEA and cost of wood tube and carbon tube, and concluded that the SEA of wood tube is approximately 1/3rd of carbon tube, and the cost of wood tube is about 1/40th of carbon tube. Gu dou et al. [33] prepared carbon fiber-wood based sandwich composite hollow components and carried out quasi-static compression tests. The results showed that the amount of absorbed energy changed linearly with the number of poplar veneers used.

Most of the previous studies focused on the quasi-static axial crushing performance of CFRP or winding GFRP composite hollow components, but not on the quasi-static axial crushing performance of BFRP-bamboo winding composite hollow components. This study aims to evaluate the axial crushing performance of BFRP-bamboo winding composite hollow components, fill the gap of axial compression performance of BFRP-bamboo winding composite hollow components, and promote its application in municipal engineering as well as civil engineering.

2 Preparation of specimen and test setup

2.1 Preparation of specimen

The bamboo winding hollow components (BT) and BFRP-bamboo winding composite hollow components (BBT) were manually produced using the following procedure. The production process of BT ca be summarized as follows: (1) The plastic wrap was bound on the PVC pipe coated with release agent; (2) The glued bamboo sheets were wrapped on the PVC pipe; (3) The processed specimens were wrapped with plastic covering; (4) After the specimen was completely cured, the PVC pipe was pulled out and the plastic covering on the surface was removed; (5) Both ends of the specimen were polished flat. The production process diagram is shown in **Fig. 2**. BBT was produced by winding BFRP on the outer surface of BT. The fiber direction of bamboo was 0 ° and the fiber direction of BFRP was 90 °.

The height of both BT and BBT was 126 mm. BT was made of 10 layers of bamboo sheets, with a single layer thickness of 0.4 mm. BBT1, BBT2, BBT3 and BBT4 were produced respectively by winding on the outer surface of BT with one layer, two layers, three layers and four layers of BFRP, resulting in different BFRP cloth ratios. The thickness of the single layer of BFRP was 0.15 mm. BFRP cloth ratio (ρ_F) is defined as the percentage of BFRP cross-sectional area in the cross-sectional area of the entire tube, and may be calculated using Eq. (1):

$$\rho_F = \frac{A_{BFRP}}{A_{tube}} \times 100\% \tag{1}$$

where, A_{BFRP} is the cross-sectional area of BFRP, A_{tube} is the cross-sectional area of the entire tube.
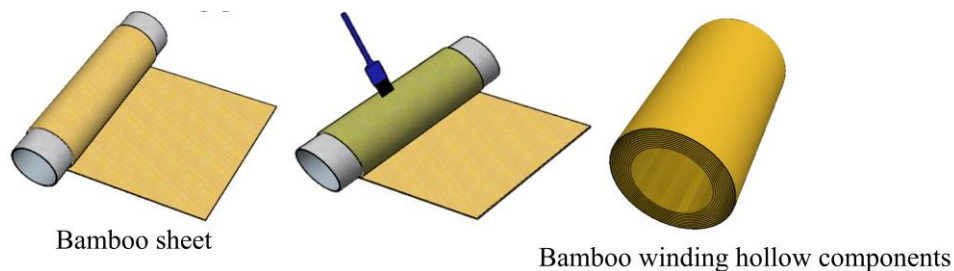

Bamboo sheet

Bamboo winding hollow components

Fig. 2. Production process of BT.

Table 1. Main parameters of specimens

Specimens	D_i (mm)	H (mm)	t_b (mm)	t_f (mm)	n_b	n_f	ρ_F (%)	Number
BT	63	126	0.4	—	10	0	0	4
BBT1	63	126	0.4	0.15	10	1	4.91	4
BBT2	63	126	0.4	0.15	10	2	8.39	4
BBT3	63	126	0.4	0.15	10	3	11.64	4
BBT4	63	126	0.4	0.15	10	4	14.68	4

Note: D_i is the inner diameter of the tube; H is the tube height; t_b is the thickness of one layer of bamboo sheet; t_f is the thickness of one layer of BFRP; n_b is the number of bamboo layers; n_f is the number of BFRP layers; ρ_F is the BFRP cloth ratio.

The current study considered 20 tube specimens, which were divided into 5 groups. The main parameters of each group of specimens are listed in **Table 1**. The specimen sizes are illustrated by taking BT and BBT1 as examples, as shown in **Fig. 3**.
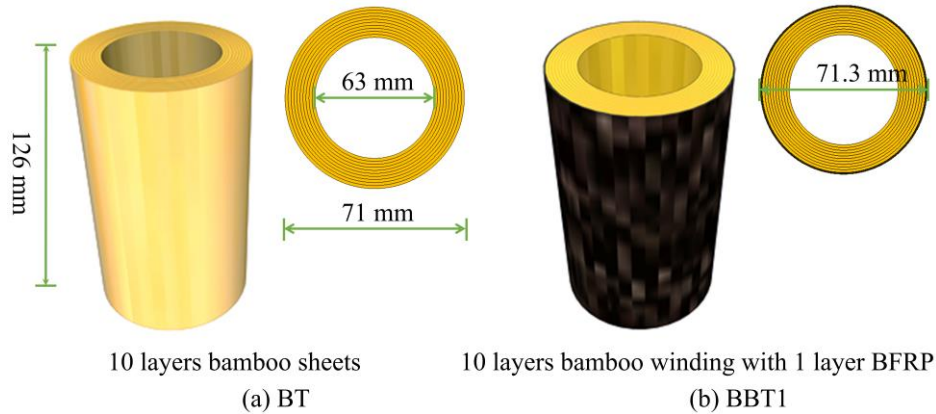

Fig. 3.   Schematic diagram showing geometric details of specimens.

The loading work of the test was completed in Jiangning Training Center of Nanjing Forestry University. The quasi-static compression test was carried out using a 50 kN universal testing machine. The specimen was placed between two rigid platens. The upper platen was used to apply compression while the lower platen remained fixed. The upper platen moved downward at a speed of 3 mm/min until the set crushing displacement was reached. Two laser displacement meters were placed at the height of the lower platen to ensure that the laser emitted by the two laser displacement meters was on the same line and passed through the axis of the specimen. The displacement data was collected by TDS-530 data acquisition instrument, and the load was controlled by the universal testing machine. A still photo camera and a video camera were placed in front of the specimen to take pictures and record the whole process of specimen crushing. The diagram of quasi-static compression test setup is shown in **Fig. 4**.
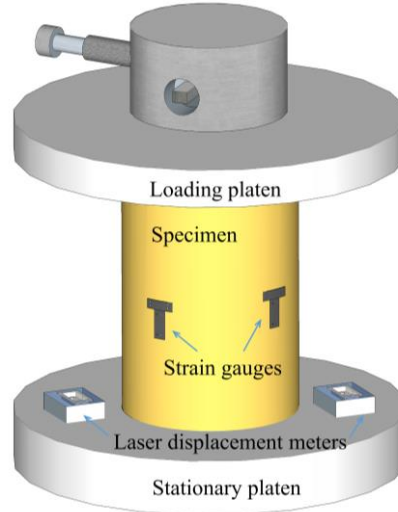

Fig. 4.   Schematic diagram of quasi-static compression test setup.

2.2 Material properties

In order to obtain the basic material properties of bamboo sheet and BFRP, dumb-bell shaped tensile specimens of bamboo sheet and BFRP were prepared, and seven repeated tests were conducted on each specimen following ASTM D3039/D3039M-14 [34]. The quasi-static tensile tests were conducted using a 50 kN universal testing machine with a loading speed of 1 mm/min. The tensile stress-strain curves of bamboo sheet and BFRP along grain direction were obtained from the test and the material properties of bamboo sheet and BFRP were calculated from the obtained data. According

to the data (**Table 2**), the tensile strength and elastic modulus of bamboo sheet were 150.17 MPa and 26 GPa, respectively, whilst those for BFRP were 987.95 MPa and 115 GPa, respectively.

Table 2. Tensile strength and tensile modulus of elasticity of specimens for material characteristics

Bamboo sheet			BFRP		
Specimens	f_b (MPa)	E_b (GPa)	Specimens	f_{bf} (MPa)	E_{bf} (GPa)
B-1	183.20	25	BF-1	941.17	86
B-2	109.38	30	BF-2	1007.61	158
B-3	121.80	21	BF-3	1091.83	110
B-4	128.84	21	BF-4	825.35	100
B-5	160.05	30	BF-5	861.98	115
B-6	176.15	27	BF-6	1103.23	100
B-7	171.79	24	BF-7	1084.45	137
Mean	150.17	26	Mean	987.95	115
COV	18.24%	13.62%	COV	10.70%	19.68%

The mechanical properties of the adhesive were provided by the manufacturer; the specified minimum values for various strength parameters are as follows: tensile strength 30 MPa, flexural strength 40 MPa, tensile shear strength 10 MPa, and compressive elastic strength 1.0×10^3 MPa [35].

2.3 Method of calculation

The evaluation indicators of energy absorption obtained from the test are as follows:

The initial peak crushing force (PCF) is the maximum force that first appears in the initial stage of crushing [27], which can be easily obtained from the load-displacement curve.

The total energy absorption (EA) is defined as the total energy dissipation of the structure during the deformation process [36], which can be calculated by integrating the area below the load-displacement curve as follows:

$$EA = \int_0^d F(x)dx \tag{2}$$

The specific energy absorption (SEA) represents the energy absorption per unit mass of the structure. SEA can be defined as the ratio of EA to the total mass (m) of the tube [37], as follows:

$$SEA = \frac{EA}{m} = \frac{\int_0^d F(x)dx}{m} \tag{3}$$

The mean crushing force (MCF) is the average value of the crushing force during axial loading [38]. It is defined as the ratio of EA to d, which is given by the following formula:

$$MCF = \frac{EA}{d} = \frac{\int_0^d F(x)dx}{d} \tag{4}$$

The crush force efficiency (CFE) is usually used to evaluate the consistency of the load, expressed as follows:

$$CFE = \frac{MCF}{PCF} \times 100\% \tag{5}$$

where, $F(x)$ is the compression load, d is crushing displacement, dx is the differential of crushing displacement, m is the total mass of specimen.

Table 3. Evaluation indicators of all groups of specimens

Specimens	EA (J)		PCF (kN)		SEA (J/g)		MCF (kN)		CFE	
	Value	Inc (%)	Value	Inc (%)	Value	Inc (%)	Value	Inc (%)	Value	Inc (%)
BT	471.18	0	23.09	0	5.91	0	5.24	0	0.23	0
BBT1	775.97	64.69	18.84	-18.40	7.96	34.80	8.62	64.69	0.46	101.82
BBT2	1105.88	134.70	16.02	-30.64	10.36	75.37	12.29	134.70	0.77	238.38
BBT3	1351.28	186.78	20.62	-10.73	10.83	83.24	15.01	186.78	0.73	221.24
BBT4	1387.04	194.37	19.12	-17.21	11.08	87.53	15.41	194.37	0.81	255.59

Note: Inc is the increase rate of energy absorption evaluation indicators compared with BT.

3 Test results

The test results are listed in **Table 3**.

3.1 Failure modes

In the process from the initial load to 70% of the initial peak load, there was no obvious crack and deformation on the surface of BT and BBT specimens. When the load reached almost to 95% of the initial peak load, BT and BBT specimens were gradually condensed and bulged outward. When the load reached the initial peak load, the bamboo fiber cracked, the BFRP was folded with audible noise of fiber fracture. With the compression process continuing, the cracks gradually expanded, and the specimen was destroyed.

According to the test process, in general, there were three failure modes for BT and BBT, **Fig. 5**.

Failure mode I: Opening. The upper bamboo fiber cracked and progressed to the lower end, causing full-length cracks as shown in **Fig. 5** (a). Such failure mode mainly occurred in BT and BBT1. The damaged BT looked like an open "petal". As for BBT1, in addition to bamboo fiber cracks, the BFRP on the outside was also torn into irregular sheets.

Failure mode II: Overall buckling. The specimen was folded and buckled at several places, resulting in overall crushing failure, as shown in **Fig. 5** (b). This kind of failure mode mainly occurred in BBT2, BBT3 and BBT4. The specimen folded in many places along the height, and the fiber folding was the most obvious in BBT4.

Failure mode III: Local buckling. Only occurred in BBT2-1. The specimen was asymmetrically inclined, the upper end was partially depressed causing the bamboo fiber to be bent and folded inward. Eventually the lower bamboo fiber was broken and the BFRP was torn, as shown in **Fig. 5** (c).
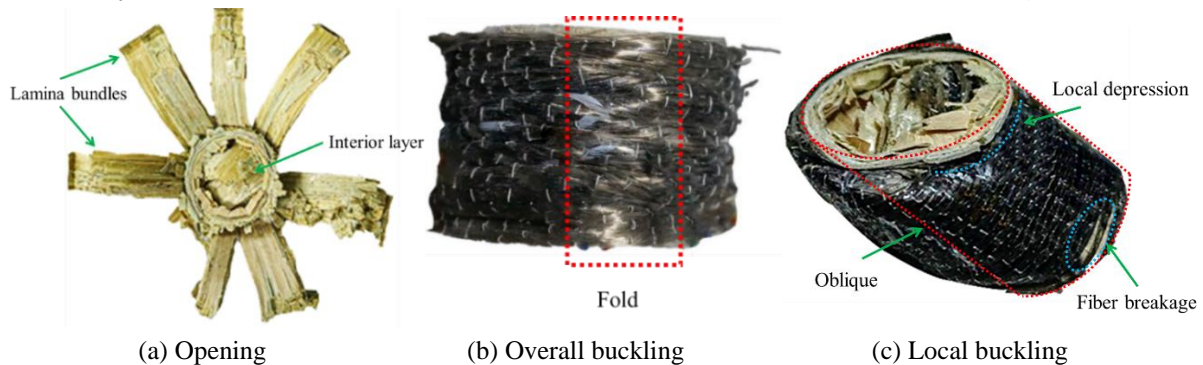

| (a) Opening | (b) Overall buckling | (c) Local buckling |

Fig. 5. Failure modes.

3.2 Load-displacement curves

The load-displacement curves of the specimens are shown in **Fig. 6**. The corresponding deformation modes are also added to each figure.

Fig. 6 (a) shows the load-displacement curves and deformation mode of BT. The deformation mode is shown by taking BT-2 as an example. BT-3 and BT-4 were similar to BT-2, and BT-1 data was not successfully collected. During the initial stage of crushing, the load increased with the increase of displacement. In the middle crushing stage, the crushing load fluctuated between 5 and10 kN, and the area enclosed below the load-displacement curve was relatively large, indicating the specimen absorbed most of the energy during this stage. In the late crushing stage, the load carrying capacity decreased, with the crushing displacement becoming smaller and the energy absorption becoming less. In the initial stage of crushing, bamboo sheets started cracking along the grain direction from the upper end. With the loading platen moving down, the specimen became flaky due to delamination cracking. Finally, the layer bundle broke, and the specimen was damaged.

Fig. 6 (b) shows the load-displacement curves and deformation mode of BBT1. The deformation mode is shown by taking BBT1-2 as an example. Other specimens in the same group were similar to BBT1-2. The shape of load-displacement curve of BBT1 was similar to that of BT. The main difference between BT and BBT1 is that the former had a large initial peak load, while the latter absorbed more

energy when it was damaged. In the initial stage of crushing, the bamboo fiber in the upper end broke in a brittle manner and the BFRP started being folded. Then the bamboo sheets became flaky due to delamination cracking and the BFRP was torn. Finally, a mixed failure mode was formed.
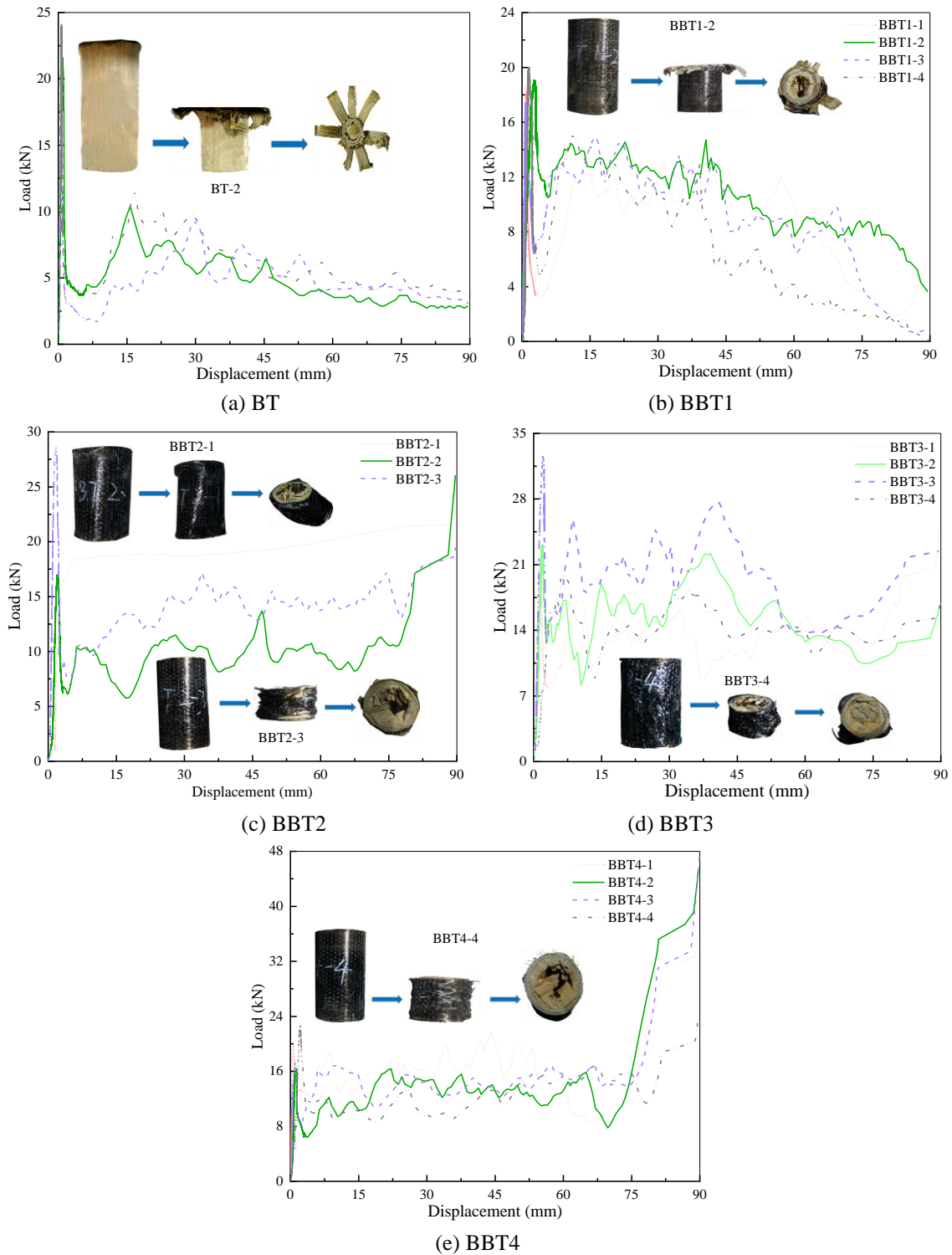

(a) BT

(b) BBT1

(c) BBT2

(d) BBT3

(e) BBT4

Fig. 6.　Load-displacement curves.

　　Fig. 6 (c) shows the load-displacement curves and deformation mode of BBT2. The deformation mode is shown by taking BBT2-1 and BBT2-3 as examples. BBT2-2 was similar to BBT2-3, and BBT2-4 data was not successfully collected. Two essentially different shapes of load-displacement curves are shown in **Fig. 6** (c). The load-displacement curve of BBT2-1 showed three-stage linearity, while the rest two curves were not completely similar to the load-displacement curves of BT or BBT1 neither.

Their differences were mainly shown in that the load carrying capacity of BBT2-2 and BBT2-3 had been greatly improved in the late crushing stage, which was due to the BFRP circumferential constraint on the radial fracture of bamboo fibers. Bamboo fibers were then forced to bend and fold inward, finally the bamboo fragments were compacted and thus improved the bearing capacity. As for BBT2-1, the crushing started from the oblique crack at the upper end, then a large plastic deformation occurred, thus it had a low load carrying capacity and a large plastic displacement; the energy absorbed by the specimen crushing was large. In general, BBT2 absorbed more energy than BT and BBT1 when damaged.

Fig. 6 (d) shows the load-displacement curves and deformation mode of BBT3. The deformation mode is shown by taking BBT3-4 as an example. Other specimens in the same group were similar to BBT3-4. The load-displacement curves of BBT3 were mostly similar to that of BBT2-3, with some difference in the middle crushing stage; the crushing load of the former fluctuated greatly and absorbed more energy. BBT3 started crushing from the upper end followed by plastic deformation. Meanwhile, specimens folded in an asymmetric mode during crushing. Finally, a mixed folding deformation mode was formed.

Fig. 6 (e) shows the load-displacement curves and deformation mode of BBT4. The deformation mode is shown by taking BBT4-4 as an example, which was similar to other specimens in the same group. The load-displacement curves of BBT4 were generally similar to that of BBT3. The main difference was that the load carrying capacity of the former was greatly improved and more energy was absorbed in the late crushing stage. BBT4 crushed from the upper end, then plastic deformation occurred, and specimens folded in an asymmetric mode during crushing. Finally, a mixed folding deformation mode was formed. It is worth noting that, compared with BBT2 or BBT3, BBT4 had the largest number of folded layers and the maximum energy absorption.

4 Results analysis

4.1 Evaluation indicators analysis

The average-load-displacement curves of each group of specimens are shown in **Fig. 7** (a), showing that the average PCF and average MCF of each group of specimens were different. The MCF from BT to BBT3 increased significantly. The MCF of BBT1 was 64.69% higher than that of BT, the MCF of BBT2 was 42.58% higher than that of BBT1, the MCF of BBT3 was 22.13% higher than that of BBT2, and the MCF of BBT4 and BBT3 were almost the same. In the fragment compaction stage, the average load carrying capacity of BBT2, BBT3 and BBT4 had been greatly improved.
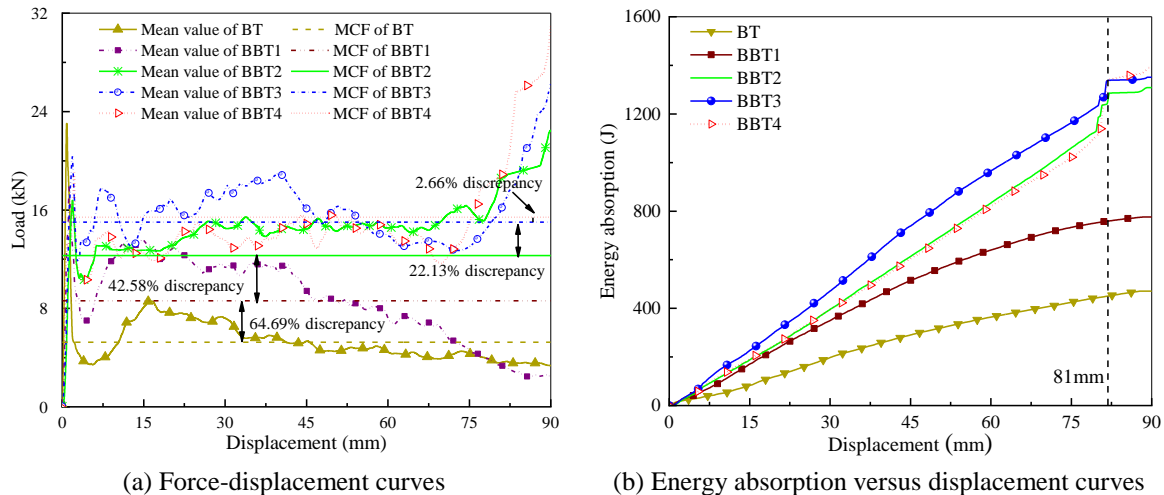

(a) Force-displacement curves   (b) Energy absorption versus displacement curves

Fig. 7. Energy absorption comparison.

The average-energy-displacement curves of each group of specimens are shown in **Fig. 7** (b). It is obvious that before the crushing displacement reached approximately 81 mm, the order of energy absorption under any displacement was BBT3> BBT2> BBT4> BBT1> BT, and the curves of BBT2 and BBT4 were extremely close. When the crushing displacement reached 81mm, the energy absorption

of BBT4, BBT3 and BBT2 signficantly increased at almost the same time. After the crushing displacement exceeded 81mm, the order of energy absorption under any displacement was BBT4>BBT3>BBT2>BBT1>BT, indicating that the BBT4 had the best energy absorption capacity in the late crushing stage.

The data of the evaluation indicators are listed in **Table 2** and are graphically shown in **Fig. 8**. It can be seen from the results that MCF, SEA and CFE generally increased with the increase of the number of BFRP layers, while PCF did not follow this trend. The PCF of BBT1, BBT2, BBT3 and BBT4 was 18.40%, 30.64%, 10.73% and 17.21% lower than those of BT, respectively. Compared with BT, the CFE of BBT1, BBT2, BBT3 and BBT4 increased by 101.82%, 238.38%, 221.24% and 255.59% respectively.
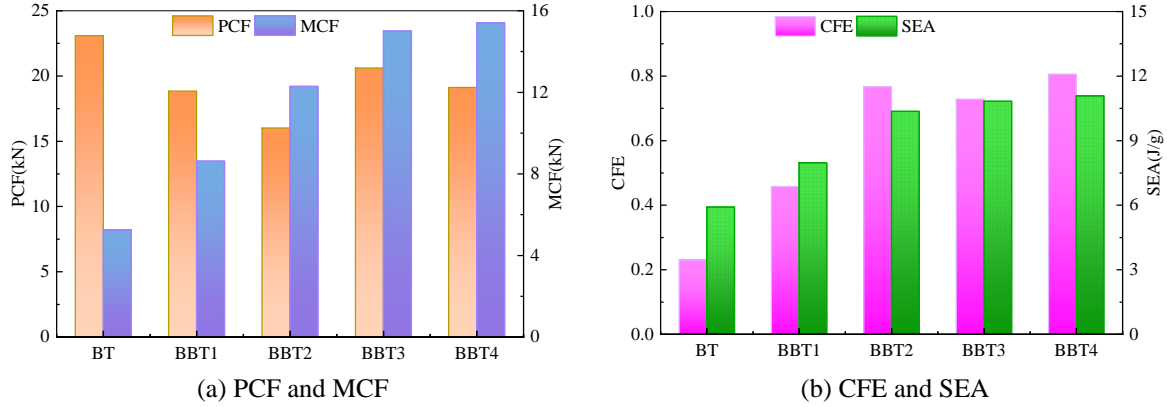

(a) PCF and MCF (b) CFE and SEA

Fig. 8. Histogram of energy absorption evaluation indicators of all groups of specimens.

Based on the obtained results, the relationships between MCF and SEA with ρ_F may be expressed by Eq. (6) and Eq. (7), respectively:

$$\frac{MCF}{MCF_0} = 1 - 0.0054\rho_F^2 + 0.208\rho_F \tag{6}$$

$$\frac{SEA}{SEA_0} = 1 - 0.0033\rho_F^2 + 0.111\rho_F \tag{7}$$

where, MCF_0 is the mean crushing force of BT specimens; SEA_0 is the specific energy absorption of BT specimens.

MCF and SEA both increased gradually with the increase of ρ_F, with the increase rate of MCF obviously faster than that of SEA. When the ρ_F reached 11.64%, i.e., 3 layers of BFRP, the increase rate of MCF and SEA remained unchanged, as shown in **Fig. 9**.
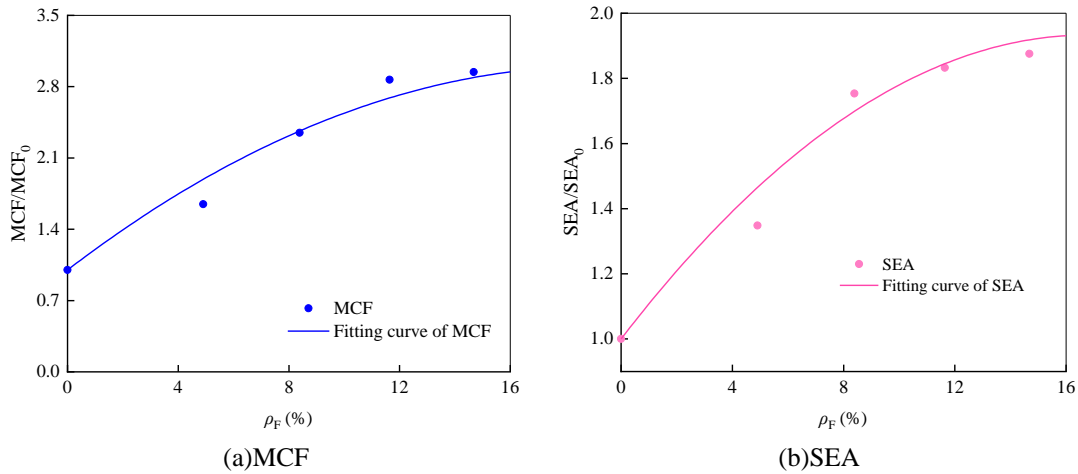

(a)MCF (b)SEA

Fig. 9. Relationship between MCF/SEA and ρ_F.

4.2 Comparison with other composite hollow components

Table 4 lists the data obtained for BT and BBT specimens as part of the current research with those of composite wrapped hollow components (CWT) and carbon reinforced composite hollow components (CRCT) reported by Praveen [39] and Huang [40]. It is obvious that for comparable dimensions, the mass of BT, BBT1, BBT2 and BBT3 are less than that of CWT and the mass of all BT and BBT specimens in the current research are significantly lower than those of CRCT. The SEA of CWT is lower than that of BBT, but the SEA of CRCT is higher than that of BBT and CWT. The CFE of both CWT and CRCT are higher than those of BT, but the CFE of BBT2, BBT3 and BBT4 are higher than those of CWT and CRCT. In summary, the specimens tested in the current study are the lightest. In terms of energy absorption, the SEA of BBT was higher than that of CWT, while the CFE of BBT specimens, especially BBT2, BBT3 and BBT4, are significantly higher than their counterparts. All these parameters clearly shows that BBT offers excellent crushing resistance.

Table 4. Comparison between data from this paper and existed studies

Specimen	Material	Composite type	$D_i \times t \times H$ (mm^3)	m (g)	SEA (J/g)	CFE (%)
BT	Bamboo	Winding	63×4.18×125.80	79.70	5.91	22.67
BBT1	Bamboo and BFRP	Winding	50×4.2×127.54	97.43	7.96	45.75
BBT2	Bamboo and BFRP	Winding	50×4.6×127	106.73	10.36	76.71
BBT3	Bamboo and BFRP	Winding	50×5.1×127.50	124.80	10.83	72.83
BBT4	Bamboo and BFRP	Winding	50×5.3×127.33	125.18	11.08	80.61
CWT1[a]	Aluminium and glass fabric/epoxy	Winding	50×150	125	6.88	57.69
CWT2[a]	Aluminium and kenaf fabric/epoxy	Winding	50×150	130	6.46	58.71
CWT3[a]	Aluminium and glass-kenaf fabric/epoxy	Winding	50×150	137	6.42	60.45
B-0[b]	Carbon fiber	Laminated	50×3.7×100	395.36	66.48	26.88
B-1[b]	Carbon fiber	Laminated	50×3.68×100	394.26	64.05	63.14
B-2[b]	Carbon fiber	Laminated	50×3.64×100	300.41	61.40	57.46

Note: t is the wall thickness of tube; m is the mass of the tube; [a] is from literature [37]; [b] is from literature [38].

5 Conclusion

A total of 20 tube specimens were produced, including BT and four types of BBT. All specimens were subjected to quasi-static axial compression by varying the cloth ratio of BFRP as an influencing factor. Moreover, the failure modes, load-displacement curves and crushing resistance of all tube specimens were analyzed. Following are the main conclusions that can be summarized based on analysis of obtained results:

(1) The quasi-static axial compression failure modes of BT and BBT were divided into three types including opening, overall buckling and local buckling.

(2) The SEA and MCF of the tube specimens increased with the increase of BFRP cloth ratio during failure. When the BFRP cloth ratio reached 11.64%, i.e., 3 layers of BFRP were wrapped outside, the increase rate of MCF and SEA remained unchanged. Compared with BT, the SEA, MCF and CFE of BBT4 increased by 87.53%, 194.37% and 255.59% respectively. Compared with other composite hollow components such as CWT and CRCT, BBT showed excellent crushing resistance despite being significantly lighter than the other materials.

Funding Statement

CRediT authorship contribution statement

HT Li: Investigation, Formal analysis, Writing – original draft, Conceptualization, Funding acquisition, Supervision. **WJ Zhou**: Funding acquisition, Investigation, Formal analysis, Writing – original draft. **BY Jian**: Writing – review & editing. **XQ Shen**: Writing – review & editing. **R Lorenzo**: Supervision, Writing – review & editing. **M Ashraf**: Supervision, Writing – review & editing.

Conflicts of Interest

The authors declare that they have no conflicts of interest to report regarding the present study.

References

[1]   Yang D, Li HT, Xiong ZH, Mimendi L, Lorenzo R, Corbi I, Corbi O, Hong CK. Mechanical properties of laminated bamboo under off-axis compression. Composites Part A: Applied Science and Manufacturing 2020; 138: 106042. https://doi.org/10.1016/j.compositesa.2020.106042

[2]   Hong CK, Li HT, Yang D, et al. Compressive performance of AFRP reinforced laminated bamboo stub columns. Archives of Civil and Mechanical Engineering 2022; 22(1): 1-12. https://doi.org/10.1007/s43452-021-00247-y

[3]   Li HT, Xuan YW, Xu B, Li SH. Bamboo application in civil engineering field. Journal of Forestry Engineering 2020; 5(6): 1-10. https://doi.org/10.13360/j.issn.2096-1359.202003001 [In Chinese]

[4]   Chen ML, Ye L, Li H, Wang G, Chen Q, Fang CH, Dai CP, Fei BH. Flexural strength and ductility of moso bamboo. Construction and Building Materials 2020; 246: 118418. https://doi.org/10.1016/j.conbuildmat.2020.118418

[5]   Lu J, Chan HL, Chen AY, Kou HN. Mechanics of high strength and high ductility materials. Procedia Engineering 2011; 10: 2202-2207. https://doi.org/10.1016/j.proeng.2011.04.366

[6]   Wu Y, Zheng Y, Yang F, Yang L. Preparation process and characterization of mechanical properties of twisted bamboo spun fiber bundles. Journal of Materials Research and Technology 2021; 14: 2131-2139. https://doi.org/10.1016/j.jmrt.2021.07.084

[7]   Chen ML, Weng Y, Semple K, Zhang SX, Hu YA, Jiang XY, Ma JX, Fei BH, Dai CP. Sustainability and innovation of bamboo winding composite pipe products. Renewable and Sustainable Energy Reviews 2021; 144: 110976. https://doi.org/10.1016/j.rser.2021.110976

[8]   Bamboo winding composite tube was invented and could be used as a high speed centrifugal yarn can. Forest Science and Technology 1959(16). [In Chinese]

[9]   Fei B, Chen M, Wang G, Ye L, Chen Q. Status and role of bamboo winding technology in National development. World Bamboo and Rattan 2018; 16(4): 1-4. [In Chinese]

[10] Wang G, Deng J, Chen F, Cheng H, Ye L. Exploitation and Application of Bamboo Fiber-Reinforced Filament-Wound Pressure Pipe. Scientia Silvae Sinicae 2016; 52(4): 127-132. [In Chinese]

[11] Chen ML, Weng Y, Semple K, Zhang SX, Hu YA, Jiang XY, Ma JX, Fei BH, Dai CP. Sustainability and innovation of bamboo winding composite pipe products. Renewable and Sustainable Energy Reviews 2021; 144: 110976. https://doi.org/10.1016/j.rser.2021.110976

[12] Li HT, Su JW, Zhang QS, Jiang, SX, Xu B, Li SH. Hollow Bamboo Biocomposite with Double-Walled Circular Structure and Preparation Method. China Patent ZL201410834875.1, application date: Dec, 2014, Authorization date: Jan. 25, 2017.

[13] Li HT, Su JW, Zhang QS, Jiang SX, Xu B, Li SH, Su SW, Guo YL. Preparation Method of Circular Composite Bamboo Cylinder Biomaterial. China Patent ZL201410837157.X, application date: Dec, 2014, Authorization date: Aug. 3, 2016.

[14] Li HT, Shen XQ, Jian BY, Zhou WJ, Corbi O. Axial compressive behaviour of transversely reinforced bamboo winding tubes. Wood Material Science & Engineering 2024; 19(2): 375-390. https://doi.org/10.1080/17480272.2023.2246942

[15] Jian BY, Li HT, Mohrmann S, Corbi O, Tian YK, Ashraf M. Research on the influence of the winding angle on the compression properties of bamboo tubular sections. Cellulose 2024; 31(12): 7335-7351. https://doi.org/10.1007/s10570-024-06015-3

[16] Castelo A, Correia JR, Cabral-Fonseca S, et al. Inspection, diagnosis and rehabilitation system for all-fibre-reinforced polymer constructions. Construction and Building Materials 2020; 253: 119160. https://doi.org/10.1016/j.conbuildmat.2020.119160

[17] Zhou WJ, Li HT, Mohrmann S, Li H, Xiong ZH, Lorenzo R. Evaluation on the axial compression mechanical properties of short BFRP laminated bamboo lumber columns. Journal of Building Engineering 2022; 53: 104483. https://doi.org/10.1016/j.jobe.2022.104483

[18] Lin JS, Wang X, Fang CQ, Huang X. Collapse loading and energy absorption of fiber-reinforced conical shells. Composite Part B: Engineering 2015; 74: 178-189. https://doi.org/10.1016/j.compositesb.2015.01.034

[19] Tarlochan F, Ramesh S, Harpreet S. Advanced composite sandwich structure design for energy absorption applications: blast protection and crashworthiness. Composite Part B: Engineering 2012; 43: 2198-2208. https://doi.org/10.1016/j.compositesb.2012.01.042

[20] Liu Q, Ma JB, He ZH, Hu Z, Hui D. Energy absorption of bio-inspired multi-cell CFRP and aluminum square tubes. Composite Part B: Engineering 2017; 121: 134-144. https://doi.org/10.1016/j.compositesb.2017.03.044

[21] Zhang ZY, Sun W, Zhao YS, Hou SJ. Crashworthiness of different composite tubes by experiments and simulations. Composite Part B: Engineering 2018; 143: 86-95. https://doi.org/10.1016/j.compositesb.2017.12.042

[22] Jin M, Yin G, Hao W, Tuo H, Yao R. Energy absorption characteristics of multi-cell tubes with different cross-sectional shapes under quasi-static axial crushing. International Journal of Crashworthiness 2020; 135: 1826825. https://doi.org/10.1080/13588265.2019.1826825

[23] Sun G, Liu T, Huang X, Zheng G, Li Q. Topological configuration analysis and design for foam filled multi-cell tubes. Engineering Structures 2018; 155: 235-250. https://doi.org/10.1016/j.engstruct.2017.11.056

[24] Zhu G, Sun G, Li G, Cheng A, Li Q. Modeling for CFRP structures subjected to quasi-static crushing. Composite Structures 2018; 184: 41-55. https://doi.org/10.1016/j.compstruct.2017.10.035

[25] Wang Y, Feng J, Wu J, Hu D. Effects of fiber orientation and wall thickness on energy absorption characteristics of carbon-reinforced composite tubes under different loading conditions. Composite Structures 2016; 153: 356-368. https://doi.org/10.1016/j.compstruct.2016.06.028

[26] Deng YB, Ren YR, Fu XW, Jiang HY. Bionic-bamboo design for enhancing the crashworthiness of composite tube with groove trigger subjected to oblique load. International Journal of Mechanical Sciences 2021; 206: 106635. https://doi.org/10.1016/j.ijmecsci.2021.106635

[27] Li SF, Guo X, Li Q, Sun GY. On lateral crashworthiness of aluminum/composite hybrid structures. Composite Structures 2020; 245: 112334. https://doi.org/10.1016/j.compstruct.2020.112334

[28] Kim HC, Shin DK, Lee JJ, Kwon JB. Crashworthiness of aluminum/CFRP square hollow section beam under axial impact loading for crash box application. Composite Structures 2014; 112: 1-10. https://doi.org/10.1016/j.compstruct.2014.01.042

[29] Zhang SX, Jiang XY, Ma JX, Sun YP, Weng Y. Ring Stiffness Test for Bamboo Winding Composite Pipe. World Bamboo and Rattan 2019; 17(04): 37-39. [In Chinese]

[30] Ma JX, Zhang SX, Sun YP, Weng Y. Bending Strength Test of Bamboo Winding Composite Pipe. World Bamboo and Rattan 2019; 17(05): 51-52+72. [In Chinese]

[31] Wei Y, Chen S, Tang SF, Zheng KQ, Wang JQ. Mechanical behavior of bamboo composite tubes under axial compression. Construction and Building Materials 2022; 339: 127681. https://doi.org/10.1016/j.conbuildmat.2022.127681

[32] Guélou R, Eyma F, Cantarel A, Rivallant S, Castanié B. Crashworthiness of poplar wood veneer tubes. International Journal of Impact Engineering 2021; 147: 103738. https://doi.org/10.1016/j.ijimpeng.2020.103738

[33] Guélou R, Eyma F, Cantarel A, Rivallant S, Castanié B. Static crushing of wood based sandwich composite tubes. Composite Structures 2021; 273: 114317. https://doi.org/10.1016/j.compstruct.2021.114317

[34] ASTM D3039/D3039M-14. Standard test method for tensile properties of polymer matrix composite materials.

[35] Li H, Li HT, Hong CK, Xiong ZH, Lorenzo R, Corbi I, Corbi O. Experimental investigation on axial compression behavior of laminated bamboo lumber short columns confined with CFRP. Composite Part A: Applied Science and Manufacturing 2021; 150: 106605. https://doi.org/10.1016/j.compositesa.2021.106605.

[36] Wang ZG, Zhang J, Li ZD, Shi C. On the crashworthiness of bio-inspired hexagonal prismatic tubes under axial compression. International Journal of Mechanical Sciences 2020; 186: 105893. https://doi.org/10.1016/j.ijmecsci.2020.105893

[37] Jin MZ, Hou XH, Yin GS, Yao RY, Gao JG, Deng ZC. Improving the crashworthiness of bio-inspired multi-

cell thin-walled tubes under axial loading: Experimental, numerical, and theoretical studies. Thin-Walled Structures 2022; 177: 109415. https://doi.org/10.1016/j.tws.2022.109415

[38] Ren YR, Jiang HY, Liu ZH. Evaluation of double- and triple-coupled triggering mechanisms to improve crashworthiness of composite tubes. International Journal of Mechanical Sciences 2019; 157-158: 1-2. https://doi.org/10.1016/j.ijmecsci.2019.06.005

[39] Praveen Kumar A, Shunmugasundaram M, Sivasankar S, Amuthavalli NK. Evaluation of axial crashworthiness performance of composite wrapped metallic circular tubular structures. Materials Today: Proceedings 2020; 27: 1268-1272. https://doi.org/10.1016/j.matpr.2019.11.093

[40] Huang JC, Wang XW. Numerical and experimental investigations on the axial crushing response of composite tubes. Composite Structures 2009; 91(2): 222-228. https://doi.org/10.1016/j.compstruct.2009.01.007